Contactless Respiration Monitoring Via Off-the-Shelf WiFi Devices

Xuefeng Liu, Jiannong Cao, *Fellow, IEEE*, Shaojie Tang, Jiaqi Wen, and Peng Guo

Abstract—Non-invasive human sensing based on radio signals has attracted numerous research interests in recent years. Previous work mainly focused on detecting the presence of a person or identifying human gestures and activities. In this paper, we show that with off-the-shelf WiFi devices, fine-grained respiration information of a person under different sleeping positions can be extracted successfully. We do this by introducing a breath monitoring system based on WiFi signals. This system adopts off-the-shelf WiFi devices to continuously collect the fine-grained wireless channel state information (CSI) around a person. From the CSI, the rhythmic patterns associated with respiration and abrupt changes due to the body movement are identified. Compared to existing respiration monitoring systems that usually require special devices attached to human body, this system is completely contactless. In addition, different from many vision-based sleep monitoring systems, it is robust to low-light environments and does not raise privacy concerns. Preliminary testing results show that our system can reliably track a person's respiration reliably in different sleeping postures.

Index Terms—Wireless technology, channel state information, breath detection

1 Introduction

It is well recognized that sleep not only affects the productivity or physical vitality of a person, but also is related to many diseases including diabetes, depression or even stroke and heart failure [1]. Therefore, a practical sleep monitoring system is highly desirable.

For a sleep monitoring system, to provide accurate respiration information is usually an important requirement. With regard to this objective, systems like the polysomnography (PSG) adopt pressure transducers or a thermocouple fitted in the nostrils to measure the airflow [2]. However, the inconvenience of these devices caused to the users make them limited to clinical settings. On the other hand, there are many types of systems that are designed to monitor one's breath in a less obtrusive or even unobtrusive manner. For example, the Tanita [3] leverages pressure sensor arrays embedded in a sleeping mat to monitor one's respiration, body motion, and even heart rate. Systems like [4] utilize cameras to track the movements of one's chest to measure the exact breathing rate. However, using pressure sensor arrays are generally expensive. Using vision-based systems like [4], on the other hand, can be negatively affected by typical low-light sleeping environment and also raise privacy concerns to the users.

- *X. Liu is with the Beijing Institute of Technology, Beijing, China. E-mail: csxfliu@gmail.com.*
- *J. Cao and J. Wen are with the Department of Computing, Hong Kong Polytechnic University, Hong Kong. E-mail: {csjcao, csjqwen}@comp.polyu.edu.hk.*
- *S. Tang is with the Jindal School of Management, University of Texas at Dallas, Dallas, TX 75080. E-mail: shaojie.tang@utdallas.edu.*
- *P. Guo is with the School of Electronic and Information Engineering, Huazhong University of Science and Technology, China. E-mail: guopeng@mail.hust.edu.cn.*

Manuscript received 27 Apr. 2015; revised 22 Sept. 2015; accepted 17 Nov. 2015. Date of publication 3 Dec. 2015; date of current version 29 Aug. 2016. For information on obtaining reprints of this article, please send e-mail to: reprints@ieee.org, and reference the Digital Object Identifier below. Digital Object Identifier no. 10.1109/TMC.2015.2504935

As a potential candidate, using RF technologies to track one's respiration has gained much attention due to the advantages of non-intrusiveness and robustness to low-light sleeping environment. The rationale behind this approach is that exhaling and inhaling causes small changes in the radio signals as they propagate from transmitter (TX) to receiver (RX). Under this category, some systems utilize special wireless devices like the Doppler radar [5], the ultra-wideband MIMO radar [6], the Universal Software Radio Peripheral (USRP) [7], and the Frequency Modulated Carrier Waves (FMCW) [8], [9]. However, these systems rely on special hardware devices, limiting the practicability in many applications.

More recently, some respiration monitoring systems based on commercial off-the-shelf transmitter-receiver are proposed. In [10] and [11], the received signal strength (RSS) measurements of a network of transceivers are utilized for extracting respiration rate. This work is improved by [12] and [13] in which the RSS data from a single TX-RX pair are able to track one's respiration rate. As an example, Fig. 1, extracted from [12], shows the original RSS measurements and the processed signal (as the dashed sinusoidal wave). The sinusoid pattern of breathing can be roughly observed in the RSS data.

Although the work in [12] and [13] show great promise of tracking human respiration using wireless radio signals, we see that there are still opportunities for further enhancements. The original RSS measurements in Fig. 1 show a stair-like pattern, indicating the low granularity of RSS to typical respiration. As a result, the RSS measurements are likely to be dominated by quantization errors and electronic noise, which lowers down the accuracy of respiration tracking (more detailed explanation about the quantization errors and electronic noise will be described in Section 3.1). To reliably identify respiration rate in the presence of noise, the respiration is assumed to be periodic [11], [12]. However, an undesirable consequence is that information like the abnormal breathing (e.g., sleep apnea) that violates the

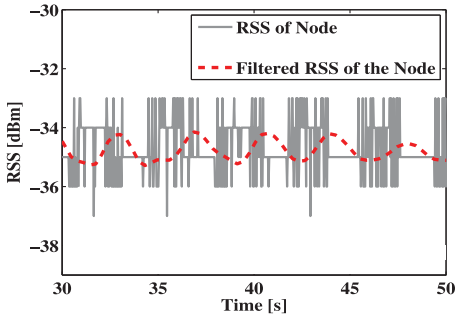

Fig. 1. The original RSS measurements and the filtered RSS. The figure is slightly modified from Fig. 5c in [11].

periodic assumption is not easily to be identified from the RSS data. In addition, the effect of the sleeping postures, and of the change of sleeping postures on the respiration monitoring have not been investigated.

These applications of using RSS measurements do enlighten us to a further step. We ask whether it is possible to find a wireless feature that is more sensitive than the RSS such that one's respiration rate can be tracked more accurately, even with un-normal breathing (e.g., sleep apnea) and in different sleeping positions.

The answer is positive. We found that the wireless channel state information (CSI) is a much more sensitive indicator than RSS for tracking one's respiration. Based on this finding, we propose a new respiration monitoring system leveraging off-the-shelf WiFi devices. This system continuously collect the CSI of the radio signals and from which extract breath information. Compared with the existing works that rely on RSS measurements, this system can track un-normal breathing (e.g., sleep apnea) and can also provide breathing information when the person is under different sleeping positions.

2 Related Works

According to the sensors adopted, existing respiration monitoring systems which are able to track human respiration can be largely divided into three categories: systems based on pressure sensor arrays, systems using camera visions, and systems based on RF signals.

Systems based on pressure sensor arrays are usually in the form of a smart sleeping mat like [14] and [3]. Such a system can provide fine-grained information like respiration, body motion, and even heart rate. However, the main drawback the high cost. For example, the price of the Tanita [3] is over 500 USD. For the camera-based systems [15] , [4], their performance can be negatively affected by low-light sleeping environment and can also raise privacy concerns. These drawbacks have lead to consistent efforts to find better alternatives.

Recently, 'taking wireless radio signals as sensors' starts to attract more and more attentions. Using RF signals for tracking respiration is based on the observation that the wireless signals, when they travel from a wireless transmitter and a receiver, can be affected by the breathing-induced chest movement on the propagation paths.

Under this category, some systems like [5] and [6], utilize special wireless devices like the Doppler radar and the ultra-wideband MIMO radar. More recently, a breathing monitoring system called Vital Radio [8], [9] uses a radar technique called FMCW. The device generates a signal that sweeps from 5.46 GHz to 7.25 GHz every 2.5 milliseconds for tracking human's breathing. All the systems above rely on specially designed hardware devices.

TABLE 1
Related Works of Using RF Signal for Respiration Monitoring

Systems	Off-the-shelf device	Tracking abnormal breathing	Under diff. sleep positions	Under chg. of sleep position
UWB [6]	×	√	–	–
Vital-Radio [8]	×	√	–	–
Wibreathe [7]	×	–	–	–
Ubibreathe [13]	√	√	√	–
COTS TX-RX [12]	√	√	–	–
BreathTaking [10]	√	√	–	–
Our system	√	√	√	√

√ (Yes); ×(No); – (Not mentioned);

On the other hand, some systems utilized commercial off-the-shelf (COTS) devices for tracking respiration. For example, the RSS measurements from a network of COTS wireless transceivers are utilized in [10] and [11]. This work is improved by [12] in which the RSS data from a single TX-RX pair are able to identify one's respiration rate. The RSS, however, is not a sensitive indicator for reliably tracking minute chest movement. Exhaling and inhaling causes very small changes in RSS and these changes can be easily polluted by other factors and environmental noise.

To address this problem, the collected RSS data are generally modelled as a sinusoid and its parameters, like the amplitude and frequency, are estimated based on a batch of RSS measurements under some certain periodic assumptions [11], [12]. However, an undesirable consequence is that abnormal breathing like sleep apnea cannot be well identified since it violates the periodic assumption. Moreover, the effect of different sleeping positions, and of the change of sleeping position during respiration monitoring have not been investigated.

In this paper, we apply CSI for respiration monitoring. We designed a series of techniques to efficiently utilize the information from the CSI data to handle different conditions, including different sleeping positions, change of sleeping positions, and sleep apnea. Table 1 compares some of the existing works of using the RF for respiration monitoring. To summarize, our system relies on the COTS WiFi devices, is able to track abnormal breathing accurately, and works well when the sleepers are at different sleeping positions or even change of sleeping positions.

3 Tracking Respiration Using WiFi Radio: Preliminary Findings and Results

3.1 Which Wireless Feature to Use?

Besides the most commonly used RSS, are there any other wireless features which are capable of tracking respiration? To answer this question, we start with some proof-of-concept experiments. We set up an experiment, in which two MicaZ nodes are deployed, one as the transmitter and the other one as the receiver. TX and RX are with 3 meters apart from each other. A person is lying on a bed in between the

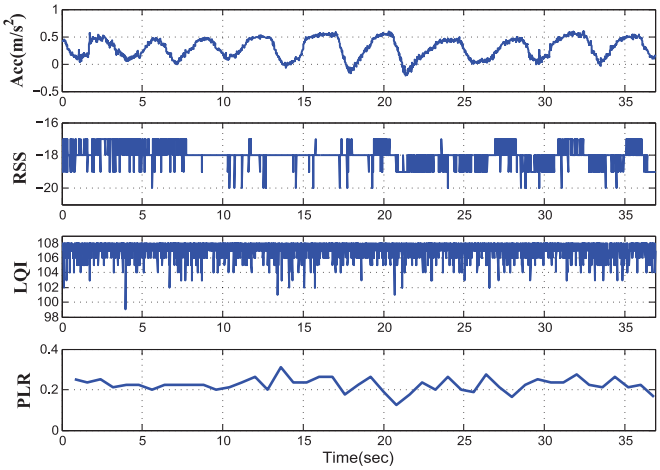

Fig. 2. Using conventional wireless features for tracking respiration. From top to bottom: (a) the acceleration data (as the ground-truth), (b) the RSS data, (c) the LQI, and (d) the packet loss rate.

TX-RX pair, breathing normally at approximately one breath (an inhalation-exhalation cycle) every 3 seconds. The TX keeps sending 100 packets per second at 1 mW transmission power. From the received packets at RX side, we extract some wireless features and try to find out how they would change with time. Here, three mostly adopted wireless features are utilized: (1) received signal strength; (2) link quality indicator (LQI); and (3) packet loss rate (PLR). Note that since PLR is a statistical quantity measuring the packet loss in a period of time, here each PLR value is calculated using data collected within a one-second window. In the meantime, we attach a smartphone on the chest of the person to track the chest movement using the embedded accelerometers. This data will be taken as the ground truth of respiration.

Fig. 2 shows the testing results. From top to bottom, the four subfigures show how the acceleration, the RSS, the LQI, and the PLR change over time. No clear rhythmic pattern of the acceleration data is shown in any of the three wireless features (although for the RSS, some patterns of breathing can be observed after 25 seconds). We then tried different location of the RX and TX and with different transmission power, but obtained similar results as shown in Fig. 2. These wireless features seem not be able to well capture the minute activities like chest movement of a person.

The major problem for these features is their low sensitivity and low resolution. Take the RSS shown in Fig. 2 as an example. The RSS values are integers, and when the person is breathing, the RSS only changes within the range between -20 to -17. This coarse-grained RSS values are reflected as stair-like pattern in Fig. 2. This observation about the RSS measurements matches well with the Fig. 1. We argue that although after some procedures like noise filtering, the SNR can be improved as in Fig. 1, the downside effect of low-sensitivity of the RSS still causes other problems mentioned in the previous two sections.

3.2 CSI for Tracking Respiration

Recently, Channel State Information has gained much attention in wireless communications [16]. CSI describes how an RF signal propagate from the TX(s) to the RX(s) and reveals the combined effect of, for instance, scattering, fading, and power decay with distance. With commodity WiFi Network

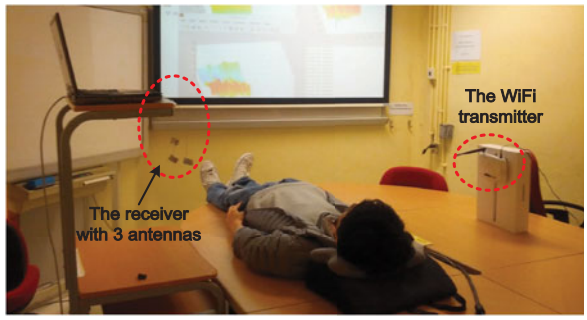

Fig. 3. Experiment setup using the CSI.

Interface Cards (NICs), a group of 30 sub-carriers' measurements can be revealed to upper layer users in the format of CSI. Each CSI depicts the amplitude and phase of a subcarrier:

$$H(f_k) = ||H(f_k)||e^{j\sin(\angle H_k)}(8), \quad (1)$$

where $H(f_k)$ is the CSI at the subcarrier k with central frequency of f_k, and $||H(f_k)||$ and $\angle H_k$ denote its amplitude and phase, respectively.

We argue that compared to the RSS, CSI is a superior metric for respiration monitoring mainly due to the following three reasons.

- *Channel response versus received energy*: The CSI is the channel response reflecting the state of wireless channels between transmitter and receiver, while the RSS is only the received energy power at the receiver side. The scattering and reflecting effects caused by minute movements of breathing will directly affect the channel state rather than the received energy.
- *Higher frequency granularity*: The scattering and reflecting effects caused by breathing can have different effect on different sub-carriers. Analyzing sub-carriers of CSI thus provides higher opportunity to capture the minute movements than using the RSS which can be regarded as the averaged power over the whole channel bandwidth.
- *Higher amplitude granularity*: The RSS is an integer with low granularity ($\pm 1\ dB$). The minute movement of breathing generally causes little changes on the RSS data. On the other hand, the CSI can provide much higher resolution in amplitude.

We start with some proof-of-concept experiments using CSI. We create a setup shown in Fig. 3 in an office at PolyU. We adopt one 802.11 compliant AP (TP Link WR740) as the transmitter and a laptop computer (Dell M2,300) using a commercial 802.11n NIC as the receiver. Note that here the NIC of the laptop has three antennas, and we extended all of them to outside (see 'the receiver with 3 antennas) for better signal quality. The transmitter sends 20 packets per second.

From each packet received, we can extract a 30-by-3 matrix called as channel frequency response (CFR) matrix. Each column of the CFR matrix corresponds to one antenna while each row corresponds to one sub-carrier. Let $CFR^j(k)$ denote the jth column of the matrix extracted from the kth packet received:

$$CFR^j(k) = [h_1^j(k), h_2^j(k), \ldots, h_{30}^j(k)]^T, \quad (2)$$

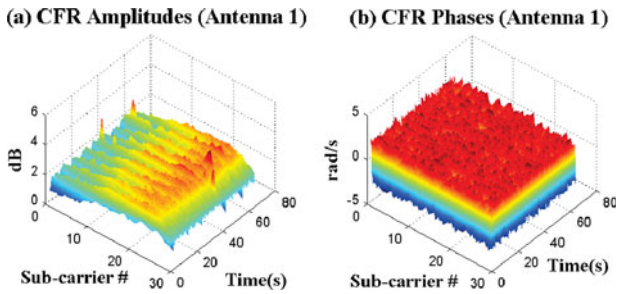

Fig. 4. The CFR amplitude and phase obtained during the experiment (antenna 1).

where $h_i^j(k)$ is the CFR on the ith subcarrier at time instant k of antenna j. Note that $h_i^j(k)$ is a complex number and is represented by the amplitude $|h_i^j|$ and the phase δh_i^j as $h_i^j = |h_i^j| * e^{j\delta h_i^j}$.

To analyze the temporal information of $CFR^j(k)$, we put together $CFR^j(k)$ collected at different time, denoted as CFR^j:

$$CFR^j = [CFR^j(1), CFR^j(2), \ldots, CFR^j(m)]. \quad (3)$$

Note that CFR^j is a 30-by-m matrix, where m is the number of packets received. Each row of CFR^j represents the temporal change of the CSI information over one subcarrier.

Fig. 4 shows the amplitude and phase of CFR^1, using data collected in 70 seconds. From the amplitudes of CFR^1, we can clearly see some ripple-like pattern, which we will shown soon corresponds to the movement of chest. On the other hand, the phase of the CFR^1 seems to be random and does not show clear correlation with breathing. Likewise, Fig. 5 shows the amplitudes of CFR^2 and CFR^3. The breathing-caused ripples can also be observed in CFR^3.

To see whether these ripples are caused by the person's chest movement, we select the CFR sequence from the tenth row from CFR^1 (i.e., the time history of the CSI information of antenna 1 at the 10th subcarrier). Fig. 6 compares the amplitude of a CFR sequence with the acceleration data recorded in the meantime. It can be seen that they exhibit strong correlation with each other.

3.3 Rational of Using CSI for Tracking a Person's Respiration

In this section, we give some intuition about why the CSI data are capable of tracking subtle movement of chest. Ideally, a wireless signal would travel directly in a straight line from its transmitter to its intended receiver. This type of propagation is known as line-of-sight (LOS). However, when an obstacle

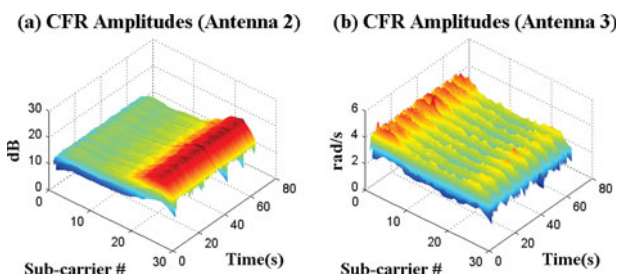

Fig. 5. The CFR amplitudes from antennas 2 and 3.

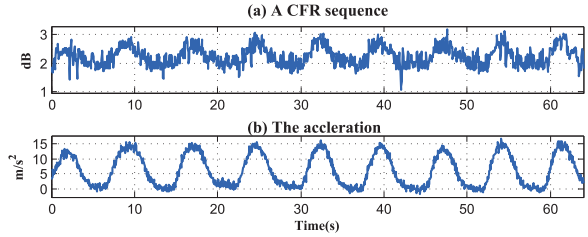

Fig. 6. (a) A comparison of the amplitude of a CFR sequence and (b) the chest movement. We can see that the two sequences closely correlated with each other.

stands in a signal's way, non-line-of-sight (NLOS) occurs and the signal can be subject to reflection, diffraction, and scattering. Obviously, during LOS and NLOS, the signal received by the receiver will have different CSI values. As shown in Fig. 7a, if, for example, the chest movement can cause a continuously shifting between LOS and NLOS, then the CSI values will show ripple-like pattern since the channel state for the LOS and the NLOS paths are significantly different.

In most conditions (including the scenario shown in Fig. 3), subtle chest movement can hardly keep generating such a shifting between LOS and NLOS. From the transmitter to the receiver, there is always a LOS path and a number of NLOS paths. When a person is breathing, the received signals can also be continuously disturbed by reflections from the moving chest. As shown in Fig. 7b, the presence of a human body would create a new reflection path while the person's breathing can repeatedly change that path. Also, a breathing person could refashion an already existing reflection path. Such changes in multi-path propagations, however, are scarcely possible to be captured by the coarse-grained RSS, yet observable through CSI.

4 Sleep Monitoring Using WiFi Radio: Advanced Findings and Results

In Section 3.2, we describe some initial results when CSI is utilized to track one's respiration. However, the scenario shown in Fig. 3 is somewhat idealistic. We summarize a few problems that deserve further study.

1) *CSI signal processing.* How to process the obtained CSI measurements such that a person's respiration can be reliably tracked? In particular, how to automatically select good CFR sequences and combine the information appropriately? These problems will be addressed in Section 4.2 and 4.3.
2) *The sleeping positions.* The person shown in Fig. 3 was laying on his back with arms at his side. Can we

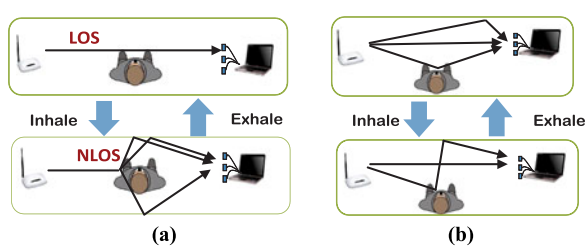

Fig. 7. Rationale of using CSI for respiration detection. (a) Breathing causes change of communication paths between LOS to NLOS. (b) Breathing causes change of communication of some NLOS paths.

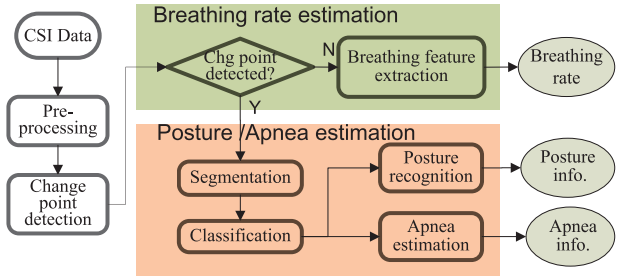

Fig. 8. The logic flow of our system.

track one's respiration when he is at different sleeping positions? Does the activity of changing sleep positions affects the performance of using CSI? Moreover, can we identify one's sleeping postures using CSI data? These problems will be addressed in Section 4.4.

3) *The ability to track abnormal breathing.* In the experiment shown in Fig. 3, the person was breathing normally during the whole experiment. Can we use the CSI to track the respiration of a person who is breathing abnormally (e.g., sleep apnea)? This question will be answered in Section 4.5.

4.1 System Overview

The architecture of the system mainly consists of two components: (1) breathing rate estimation under typical sleeping conditions, and (2) sleep posture detection and apnea detection. As shown in Fig. 8, our system works as follows. The raw CSI measurements are passed through the preprocessing unit in which the noise and outliers are removed. Afterwards, the CSIs are analyzed to decide whether there are some changes occur in the CSI data which can be attributed to the facts other than breathing (i.e., sleep apnea and change of sleeping positions). If the answer is NO, breathing rate will be estimated. Otherwise, the data are further analyzed to see whether the change of CSIs is caused by the change of sleeping postures, or by the sleep apnea. The corresponding information will be provided accordingly.

In the following sections, we will first introduce how the CSI data are pre-processed (Section 4.2). Then we introduce how the breathing rate is estimated under typical sleeping conditions (Section 4.3). Furthermore, the effect of sleeping postures, and how to track breathing under the change of sleeping postures are introduced in Section 4.4. At last, we will describe how to track abnormal breathing in Section 4.5.

4.2 CFR Data Pre-Processing

Based on the findings shown in Fig. 4, the amplitude of the CFR data will be taken as the input for monitoring one's respiration. In this section, we describe how the CFR can be processed for tracking respiration better.

Outlier removal. The first step to process a CFR sequence is to remove outliers. We found that in the collected CFR sequences, there are some abrupt changes of CFR amplitudes that are obviously not caused by the movement of chest. Fig. 9a shows the CFR from all the 30 sub-carriers of antenna 1. It can be seen that near 22, 28 and 30 s, there are some significant abrupt change points of the CFR in some or all the sub-carriers. We can also see some similar change points in Fig. 4. These are outliers and must be eliminated.

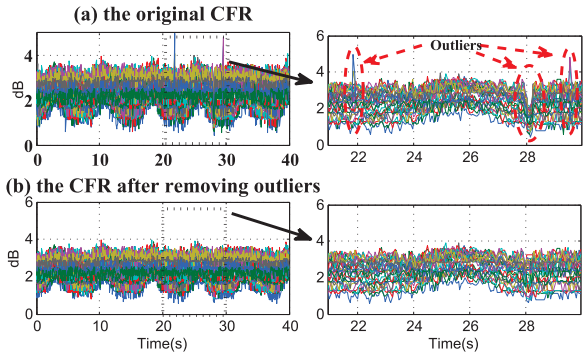

Fig. 9. (a) The original CFR from all the 30 sub-carriers of antenna 1. Left: all the time span (from 0∼40 seconds. Right: selected time span (from 20 ∼ 30 seconds. (b) The CFR after the outliers are removed using the Hampel filter.

We utilize the Hampel identifier [17], which declares any point falling out of the closed interval $[\mu - \gamma * \sigma, \mu + \gamma * \sigma]$) as an outlier, where μ and σ are the median and the median absolute deviation (MAD) of the data sequence, respectively. The reason why we choose median and MAD instead of commonly used mean and standard deviation is because the latter two parameters are sensitive to the presence of outliers in the data. We apply the Hampel identifer on all the 30 sub-carriers. The Hampel identifier adopted here has the window size of 20 data points, which means that each time, recently collected 20 data points will be processed to remove outliers. In addition, the standard threshold $\gamma = 3$ is adopted. Although this threshold can be determined by some preliminary measurements, we adopt the standard one because results show that it can gracefully apply to various environments.

Fig. 9b shows the results after all the identified outliers have been removed. We can see that the Hampel identifier performs very well in this scenario.

Interpolation. In our previous experiment, although the transmitter is programmed to transmit packets every 50 ms, we cannot guarantee the receiver is able to get one packet with the same frequency. We found that sampling jitter is quite common and sometimes can reach more than 300 ms. Jitters are caused by packet loss, or due to the Linux system on the APs which lacks support for the users to arbitrarily prioritize high-level tasks. Therefore, the CFR signal should be interpolated. We utilize linear interpolation to obtain the CFR samples at the a universe sequence of evenly spaced time points, with 50 ms apart between consecutive values.

Noise filtering. After interpolation, the noise contained in the CFR data should be eliminated. We argue that it is not appropriate to use conventional filters (e.g., the Butterworth and Chebyshev filters) to remove high frequency noise contained in the CFR. This is because they not only smooth away noise but also blur the rising/falling edges that possibly appeared in CFR signals, which is however critical for detecting sleep apnea and rollovers. Here, we apply the wavelet filter proposed in [18] since it can preserve extremely well the sharp transitions in signals than the other low-pass filters . To be more specific, we apply four-level 'db4' wavelet transform on each CFR sequence and use only the approximation coefficients to 're-construct' the filtered signal. As an illustration, Figs. 10a and 10b show all the 30 CFR sequences before and after using the wavelet

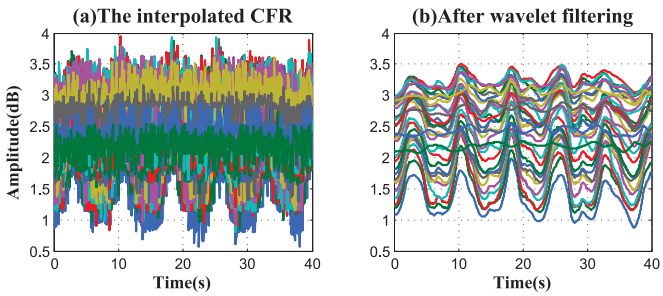

Fig. 10. (a) The interpolated 30 CFR sequences before using the wavelet filter. (b) After using the wavelet filter.

filtering. It can be clearly seen that the original noisy CFR signals becomes much cleaner.

4.3 Tracking Respiration in Typical Conditions

In this section, we describe how to track one's breathing in typical conditions. Here, typical conditions are defined as those shown in Fig. 3, in which a person is sleeping on the back and breathing normally.

In the following two sections, we will first describe how to accurately estimate the respiration rate given a single CFR sequence. Then we introduce how the multiple CFR sequences from different sub-carriers can be combined to obtain a better result. For example, in Fig. 6, the 10th sub-carrier is selected for respiration monitoring. Is there any way to select good CSI sub-carriers and combine their information efficiently for tracking chest movement? We will answer the question in the following two sections.

4.3.1 *Breathing Rate Estimation Based on Individual CFR Sequence*

For a CFR sequence, we can obtain the respiration rate by performing a short-time Fourier transform (STFT). The idea of the STFT is to divide a time signal into shorter segments and then compute the fast Fourier transform (FFT) on each segment. The STFT can real how frequency content of a signal changes with time and therefore is adopted here for tracking respiration. The breathing rate within a segment can be identified as the location of the peaks of the FFT. For example, Fig. 11 shows the FFT of a CFR sequence over a 40-second window, and the identified breathing rate is 0.125 Hz.

However, using the above approach usually suffers from the low frequency resolution. The CFR sequence in Fig. 11 contains data of 40 seconds, which leads to the 0.025 Hz frequency resolution. A larger time duration can provide higher frequency resolution but will decrease time resolution, making the system less capable of tracking changes in breathing rate. To handle this problem, instead of using the FFT peak, we adopt the method proposed in [19] and [8] to estimate the breathing rate. For each segment, we first implement the FFT but keep only the peak and its two adjacent bins. Afterwards, we perform an inverse FFT to obtain a complex time-domain signal. The phase of the signal will be linear and its slope will correspond to the breathing rate.

As a result, Fig. 11 shows that using the above method, the respiration rate is 0.133 Hz, which represents a higher frequency resolution and more accurate than the FFT method.

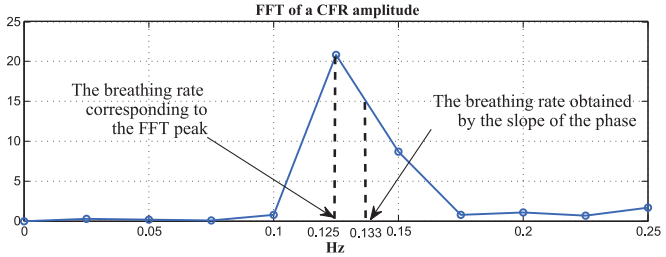

Fig. 11. The FFT of the amplitude of a CFR sequence. The location of the peak is the breathing rate (0.125 Hz). This is however a coarse estimation of the breathing rate considering the frequency resolution is only 0.025 Hz. However, using the method proposed in [19], a more accurate respiration rate (0.133 Hz) is obtained.

4.3.2 *Embracing Frequency Diversity*

In the previous section, we estimate the respiration rate using the CFR sequence from a single sub-carrier. In this section, we will show how to combine the information from different sub-carriers to obtain a better result.

Due to frequency-selective fading, the breathing motion will cause different extents of signal perturbation on different sub-carriers. As can be seen from Fig. 10b, not all the CFR sequences show the pattern of breathing equally well. For example, Fig. 12a shows five CFR sequences from sub-carriers $\#1, \#5, \#15, \#25, \#30$. We can see that some of CFR sequences, particularly for sub-carrier $\#30$ (signal shown in the middle of Fig. 12a), do not contain as much information of breathing as others. Considering that the breathing motion may have little effects on a specific sub-carrier, utilizing the information from multiple sub-carriers would potentially improve the accuracy as well as the reliability of breathing rate estimation.

For the CFR sequence of each sub-carrier, we can obtain a respiration rate. For the 30 sub-carriers, we therefore have $\mathbf{f}_e = \{f_1, \ldots, f_{30}\}$, with f_i corresponding to the estimate from the ith sub-carrier. Ideally, all the elements in $\mathbf{f}_e$ should be the same. However, due to the noise caused by selective fading, the breathing rate is different from different subcarriers.

To take the advantage of multiple sub-carriers, we first remove the outliers in $\mathbf{f}_e$ using the modified Z-score test [20]. The modified Z-score of each f_i is defined as

$$Z(f_i) = \frac{0.7645(f_i - median(\mathbf{f}_e))}{median(|\mathbf{f}_e - median(\mathbf{f}_e)|)}. \quad (4)$$

It is recommended in [20] that the modified Z-scores with an absolute value of greater than 3.5 be labeled as outliers.

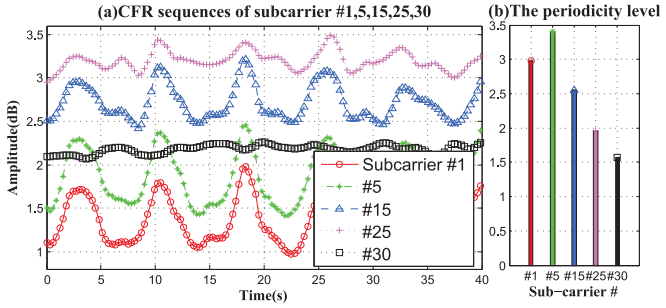

Fig. 12. (a) The CFR sequences from subcarrier $\#1, \#5, \#15, \#25, \#30$. (b) The corresponding periodicity level of the five CFR sequences.

For the remaining elements after the Z-score test, the weighted median is utilized as the final estimate of breathing rate. Assume we have n distinct elements $f_1, f_2, \ldots, f_n$ with positive weights $w_1, w_2, \ldots, w_n$ such that $\sum_{i=1}^{n} w_i = 1$, the weighted median is the element f_k satisfying: $\sum_{f_i < f_k} w_i < 1/2$ and $\sum_{f_i > f_k} w_i \leq 1/2$.

The reason why we choose the weighted median here is because it allows for non-uniform statistical weights related to varying precision measurements in the sample. Considering CFR sequences for different sub-carriers are affected differently by the respiration, they should be weighted differently for final respiration rate estimation. Considering the movement of chest shows rhythmic patterns, *f_is estimated by the CFR sequences with higher level of periodicity should be given higher weights*. How to determine the weight w_i for each CFR sequence will be described in detail in the next section.

4.3.3 Quantifying the Periodicity of the CFR Data for Different Sub-Carriers

To quantify the periodicity of a CFR sequence, we first model the sequence as a sinusoidal wave. Then the ratio of the two parameters, the amplitude of the sinusoid, and the goodness of fit of the sinusoid, are utilized to calculate the periodicity level. The justification is as follows. First, if a CFR sequence can be accurately modelled as a sinusoidal wave, then we regard it as with a high periodicity level. Second, we argue that the larger the amplitude of the identified sinusoidal wave, the higher the periodicity level.

When a person is breathing, a measured CFR sequence $x(t)$ can be largely modelled as a sinusoidal wave:

$$x(t) = Asin(2\pi ft + \phi) + D + \epsilon(t), \tag{5}$$

where the constants A, f, ϕ and D are the amplitude, frequency, phase, and shift of the identified sinusoidal wave, and $\epsilon(t)$ is an additive noise.

Given $x(t)$, the parameters of the sinusoidal wave (A, f, ϕ and D) can be identified using the Nelder-Mead method [21], which is a common non-linear optimization technique for multidimensional unconstrained minimization. Here, considering the frequency f has already been estimated using the method described in Section 4.3.1, we regard f as a known constant when applying the Nelder-Mead method.

The goodness of fit can be calculated by the root-mean-square error (RMSE) defined as

$$RMSE = \sqrt{\frac{\sum_{t=1}^{n} (\hat{x}(t) - x(t))^2}{n}}, \tag{6}$$

where $\hat{x}(t)$ is predicted values at time t using the sinusoidal model and n is the length of the $x(t)$. Based on the $RMSE$ and A, we define the periodicity level of a $x(t)$, denoted as p_r, as the ratio of the two parameters:

$$p_r = \frac{A}{RMSE}. \tag{7}$$

Obviously, the greater the p_r, the higher the periodicity of a CFR sequence.

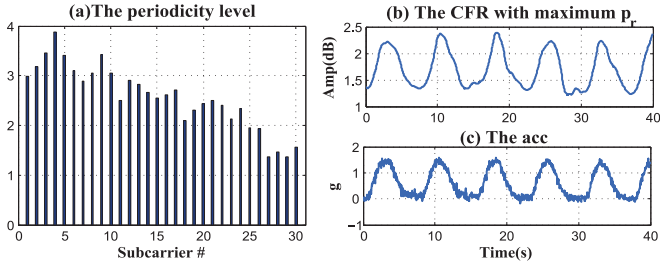

Fig. 13. (a) The periodicity level of 30 CFR sequences. (b) The the CFR sub-carrier with maximum p_r (i.e., Sub-carrier $\#4$). (c) The corresponding acceleration data.

As an illustration, Fig. 12b depicts the value of p_r of the five CFR sequences shown in Fig. 12a. It can be seen that the CFR sequences from the first three sub-carriers (i.e., $\#1, \#5, \#15$) have greater p_r than the remaining two. This matches well with the observation that these three CFR sequences look more periodic than others.

Fig. 13a shows the periodicity level of all the 30 CFR sequences shown in Fig. 10b. Moreover, Fig. 13b shows the CFR from the sub-carrier $\#4$, which has the maximum p_r. To see this CFR sequence contains more breathing information, Fig. 13c shows the corresponding acceleration data. It can be seen that the CFR from this sub-carrier shows high correlation with the breathing-induced motion. This observation justifies that the obtained respiration rate from the sub-carriers with higher periodicity level should be assigned with higher weights for respiration monitoring.

Having obtain p_r for a sub-carrier i, the w_i for the frequency estimate of this sub-carrier is calculated as:

$$w_i = \frac{p_r^i}{\sum_{i=1}^{n} p_r^i}, \tag{8}$$

where p_r^i is the p_r for the ith sub-carrier.

Also should be noted is that p_r is utilized not only for estimating the weight of f_i for breathing rate estimation, it is also taken as a feature for identifying the sleeping postures and sleep apnea. This part will be described in the next two sections.

It is interesting to see what affects the periodicity of each sub-carrier. After a number of experiments, we found that if we fix the placement of TX-RX pairs and let the sleeper stay in a certain position, the periodicity of each sub-carrier generally remains stable with time. However, when the location of TX-RX pair or the location of sleeper changes, the periodicity of sub-carriers will change accordingly. After analyzing, we believe this is because the change of location of TX-RX/sleeper will cause the change in certain multi-path components, which as a consequence, will lead to the change of frequency-selective fading [16]. As a result, the periodicity of sub-carriers will change accordingly.

4.4 Tracking Respiration at Different Sleeping Positions

In this section, we will describe the effect of sleeping positions and how to track respiration in different sleeping positions.

4.4.1 The Effect of Sleeping Positions

In the previous section, we describe how to track respiration when one is laying on the back. In this section, we will study

Fig. 14. The most popular sleeping positions. From left to right: Foetus, Log, Yearner, Solider, Freefaller, and Starfish. (The figure is from [22]).

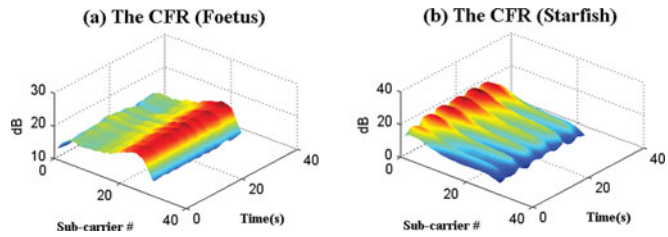

Fig. 15. The results of the system for sleeping positions (a) 'Foetus' and (b) 'Starfish'. The respiration can be much better tracked when the person is at 'Starfish' position.

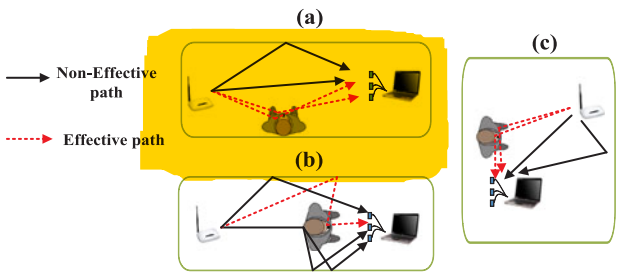

Fig. 16. (a) For sleeping positions like the 'Soldier' and 'Starfish', there are many effective paths which carry information of chest movement. (b) For sleeping positions like 'Foetus', 'Log', and 'Yearner', the number of 'effective paths' is much smaller. (c) By changing the positions of the TX-RX pair, the number of effective paths can be increased.

the effect of sleeping positions. For simplicity, we still assume the person breathes normally.

Fig. 14 shows six most common sleeping positions [22]: (1) Foetus : Sleeping all curled up into a ball with knees drawn up and chin tilted down. (2) Log: On side, arms at sides. (3) Yearner: On side, arms out. (4) Soldier : On back, arms at sides. (5) Freefaller: Face down. (6) Starfish: On back, arms up.

We test the system when the person is at different sleeping positions. In particular, the TX and the RX are placed at two sides of the person (as shown in Fig. 3) and the person is breathing normally for about 10 minutes.

As an example, Fig. 15a shows, when the person is in the 'Foetus' position, the processed CFR sequences of all the 30 sub-carriers in a 30-second period. Similarly, Fig. 15b shows the corresponding results of the 'Starfish' position. Obviously, the respiration can be much better tracked when the person is at 'Starfish' position.

What causes the problem? We believe it is caused by the 'mis-match' between the location of the TX-RX pair and the person's sleeping position. In these experiments, the TX and the RX are placed at different side of the human body. As shown in Fig. 16a, for the sleeping positions like the 'Soldier' and 'Starfish' in which the person is facing upward, there are many NLOS paths that carry information

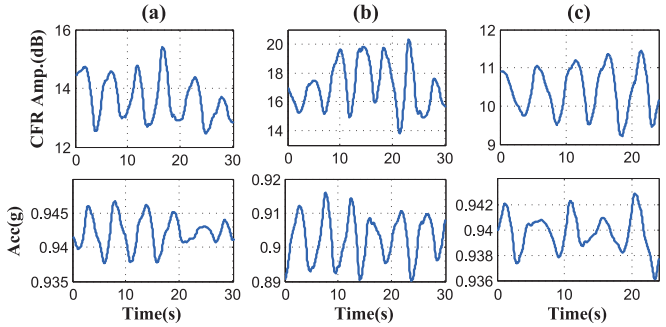

Fig. 17. The results of the system for sleeping positions 'Foetus', 'Log', and 'Yearner' after TX-RX pair has put at the same side of the person's chest. (a) The CFR amplitude from the CFR sequence with the maximum p_r (upper figure) and the corresponding acceleration (lower figure) for the 'Foetus' position. (b) The CFR and the acceleration for the 'Log' position and (c) for the 'Yearner' position.

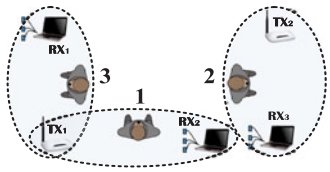

Fig. 18. Three pairs of TX-RX collaboratively work to monitor the respiration of a person. TX_1 and RX_1 work when the person is sleeping on his left side. TX_1-RX_2 work when the person is sleeping on his back, and T_2-R_3 are utilized for the right-side sleeping positions.

of the chest movement. These *'effective paths'* are generated when the wireless signal sent from the TX is reflected from the chest. In this condition, respiration can be well captured using the CSI information. However, for the 'Foetus', 'Log', and 'Yearner' in which the person is sleeping on one side (see Fig. 16b), the number of effective paths is much smaller, and the performance will be degraded.

To be able to better track the chest movement under 'Foetus', 'Log', and 'Yearner', we need to change the position of the TX-RX pair such that the number of effective paths can be increased. This can be achieved by placing both the TX and the RX at the same side of the person's chest, as shown in Fig. 16c.

As an illustration, Fig. 17 shows the results after TX-RX pair has put at the same side of the person's chest. Specifically, Figs. 17a, 17b, and 17c show the CFR sequence with the maximum periodicity for the sleeping positions 'Foetus', 'Log', and 'Yearner', respectively. It can be seen that with change of the location of the TX-RX pair, the performance of the system is significantly improved.

Therefore, we argue that to be able to reliably track a person's breathing, it is preferable to have three TX-RX pairs. As shown in Fig. 18, the first pair, consisting of transmitter 1 (TX_1) and the receiver 1 (RX_1), is placed at the left side of a person to track his respiration when he sleeps on his left side. The second pair, TX_1-RX_2, is utilized when he sleeps on his back. Note that these two pairs share the same TX_1. This can be achieved by letting TX_1 broadcast WiFi signals that can be received by both RX_1 and RX_2. The third pair TX_2-RX_3, is placed at the right side of the person to track the respiration when he is sleeping at the right side. It should be noted that we cannot eliminate RX_3 by letting RX_2 alternatively receive WiFi signals from TX_1 and TX_2 because the handoff usually takes a few seconds.

TABLE 2
Test Scenarios when the Person Changes His Sleeping Positions

Stage #	Time duration	Sleeping position
Stage 1	$0 \sim 82s$	Slept on his back
Stage 2	$83 \sim 110s$	Slept on his left side
Stage 3	$111 \sim 148s$	Slept on his back
Stage 4	$149 \sim 175s$	Slept on his right side
Stage 5	$176 \sim 201s$	Slept on his back

4.4.2 Exploring the Periodicity Level of CSI Data for Sleeping Position Estimation: The Initial Observation

Considering different TX-RX pairs perform differently for different sleeping positions, we therefore need to first find out one's sleeping position and then select the corresponding TX-RX pair. Here for simplicity, we classify six sleeping positions shown in Fig. 14 into three categories: sleeping on one's back, sleeping on one's left side and sleeping on one's right side.

To gain some insight of how to utilize CSI for identifying sleeping positions, we carried out an experiment in which a person in Fig. 18 changed sleeping positions a few times shown in Table 2. The locations of three TX-RX pairs are the same with those shown as in Fig. 18.

Figs. 19a, 19b, and 19c show the CFR data from TX_1-RX_1, TX_1-RX_2, and TX_2-RX_3, respectively. We can see that during Stage #1 ($0 \sim 80s$), data from TX_1-RX_2 show more salient periodic pattern of breathing than the other two pairs. On the other hand, when the person rolled over to the left side at Stage #2 , data from TX_1-RX_1 show the strongest periodicity. We can see that for a certain sleeping position, the CFR data placed at an *appropriate* position are likely to show the strongest rhythmic pattern (i.e., TX_1-RX_2 for sleeping on ones' back, TX_1-RX_1 for sleeping on the left side, and TX_2-RX_3 for sleeping on the right side). This conclusion can also be applied to the remaining three stages shown in Fig. 19. Therefore, a simple approach to identify sleeping position is to see which TX-RX pair has the CFR data with the strongest periodicity level.

In real situations, however, this approach does not utilize the information from the remaining two TX-RX pairs. To improve the reliability, we devise PET, a PEriodicity

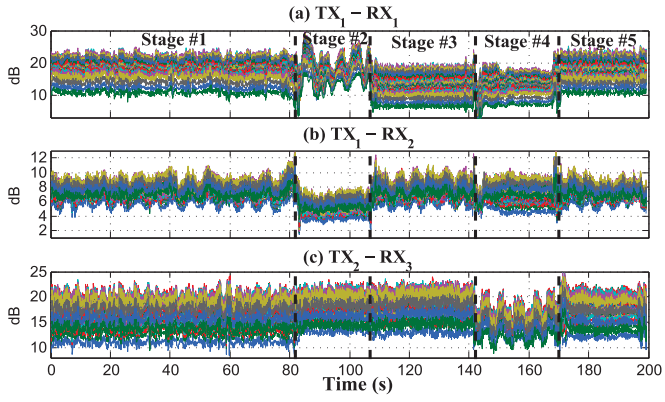

Fig. 19. The measured CFR data from three TX-RX pairs when a person slept in a few positions shown in Table 2. (a) From the pair TX_1-RX_1. (b) From the pair TX_1-RX_2. (c) From the pair TX_2-RX_3. Each subfigure shows the CFR data from 30 sub-carriers.

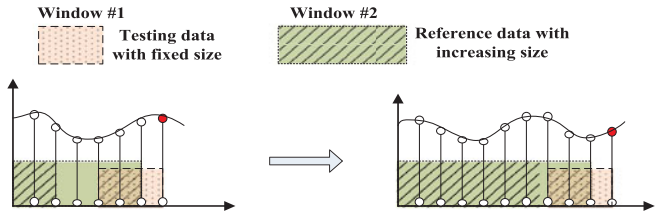

Fig. 20. Using the sliding window to detect change point. The testing data are in a running window with fixed size (window #1), while the reference data are in an increasing-sized window with left point anchored at the start of the segment (window #2). When window #1 is moving from left to right, data in the window are compared with those in window #2. A change point is detected if data in these two windows have different distribution.

Topography-based method that leverages data from three TX-RX pairs to identify sleeping position. A certain sleeping position has been recorded over three TX-RX pairs with different periodicity level (represented as a periodicity vector). Accordingly, each sleeping position will have a unique periodicity signature (or topography) over three TX-RX pairs. These TX-RX pairs can collaboratively build a topography database a priori, and we can identify a sleeping position by matching a newly measured periodicity vector with the topography database.

4.4.3 Exploring the Periodicity Level of CSI Data for Sleeping Position Estimation: Change Point Detection and Segmentation

However, to implement the PET when every single data sample is received is not advisable, as the evaluation of the periodicity level is more reliable given enough amount of data. A better approach is therefore to first divide the CSI data into segments where data in every segment come from the same sleeping position. Then the PET is carried out for each segment. The correct segmentation can be achieved based on the changing points contained the CSI data.

To detect change points in the CSI data, we design a sliding-window algorithm illustrated in Fig. 20. The basic idea of this algorithm is to search from left to right, whether the data in a sliding window have the same distribution with the proceeding data. More specifically, we have two windows. The window #1 , containing a portion of new data to be tested, is a running window with fixed size. The window #2, containing the reference data, has a increasing window length with the left point anchored at the start of the segment. Firstly, the left side of the window #2 is fixed at the first data point of a CSI time series, which is assumed to the start of the first segment. Then window #1 is moving from left to the right (see Fig. 20). At each point, we test whether data in window #1 have the same distribution with those in window window #2. If the answer is positive, then the window #1, along with the right side of window #2, move one step to the right. Otherwise, we declare a changing point is detected and we anchor the left point of the window #2 to this new point. In this paper, the size of the window #1 is 100, which corresponds to 5-second data.

When testing whether data in window #1 have the same distribution with those in window #2, we utilize the Kolmogorov-Smirnov test (KS test) [23]. To alleviate the effect of non-normal distribution, data in both windows are divided into subgroups and for each subgroup we calculate the

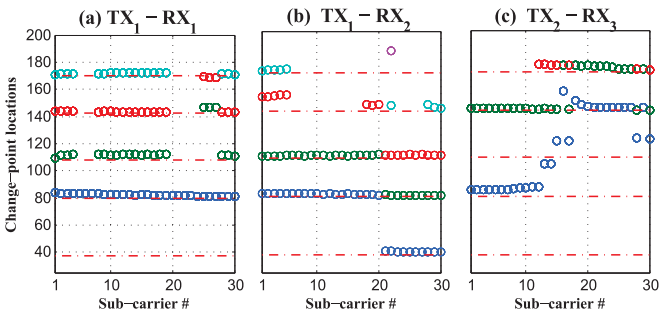

Fig. 21. The change points respectively detected from (a) TX_1-RX_1, (b) TX_1-RX_2, and (c) TX_2-RX_3. The dashed horizontal lines are the finally obtained change points using the DBSCAN method.

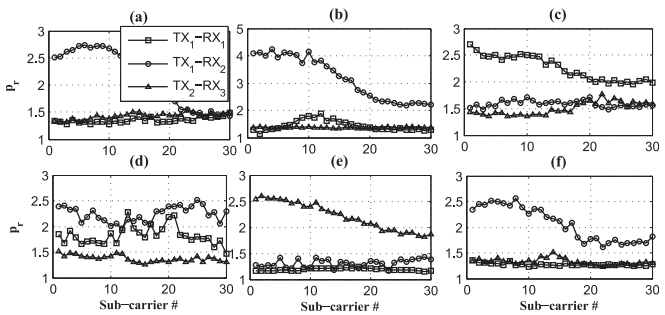

Fig. 23. (a)∼(f): The periodicity level of data segment $\#1 \sim \#6$ shown in Fig. 22. Each sub-figure shows the periodicity level of the corresponding data segment from three TX-RX pairs at all 30 sub-carriers.

average. According to the central limit theorem [24], the average will follow the normal distribution. The KS-test generates the p-value, and we require that if the p-value is smaller than 0.5, we have enough confidence to reject the null hypothesis and a changing point is detected.

Note that the above change point detection is carried out for every CFR sequence. Figs. 21a, 21b, and 21c show the change points detected using the 30 CFR sequences from TX_1-RX_1, TX_1-RX_2, and TX_2-RX_3, respectively. It can be seen that the change points identified in these three TX-RX pairs are not completely the same. Even for the same TX-RX pair, the change points from 30 sub-carriers are generally different. Also note that some outliers can be observed, especially in Fig. 21c. To obtain reliable change points, we utilize the DBSCAN [25], a k-mean clustering method with the capability to remove outliers. The center of each cluster generated by the DBSCAN is taken as a change point. The finally obtained 5 change points are shown as the dashed horizontal lines in the Fig. 21.

Using the obtained five change points, the CSI data from all three TX-RX pairs are divided into six segments and are shown in Fig. 22. Compared with the 'ground truth' shown in Fig. 19, we can see that all the change points have been successfully detected. There is one 'false-positive' change point located near 40s. This false positive change point, however, will not affect the result of identifying sleeping postures.

4.4.4 *Exploring the Periodicity Level of CSI Data for Sleeping Position Estimation: Put it Together*

Having obtained the change points, we then calculate the periodicity vector for each segment. Figs. 23a, 23b, 23c, 23d, 23e, and 23f show the periodicity level of data segment $\#1 \sim \#6$ in Fig. 22, respectively.

Take Fig. 23a as an example. It shows the periodicity level of the first data segment (i.e., $0 \sim 38s$) from three TX-RX pairs. Two observations are noteworthy. First, for a TX-RX pair, the periodicity level of its 30 sub-carriers can vary significantly. Second, despite of the internal variance, the periodicity level of the TX_1-RX_2 is on average the highest among three TX-RX pairs. This matches our expectation since the pair is at the appropriate location for the current sleeping position (sleeping on one's back). These two observations can also be found in the remaining five sub-figures.

To find out the periodicity features required in PET, we need to obtain an overall periodicity measure for each TX-RX pair. For a certain TX-RX pair, we sort the periodicity levels from all its 30 sub-carriers in the descending order, and take the average of the first 10 as its overall periodicity measure. By removing information from sub-carriers with low periodicity, this approach can be resilient to outliers. As a result, Fig. 24 shows the finally obtained periodicity vectors for all six data segments. For the first two segments when the person is sleeping on this back, the periodicity vectors are similar in the sense that they have the largest element in the middle (corresponding to TX_1-RX_2), the second largest at the right (TX_2-RX_3), and the lowest at the left (TX_1-RX_1). This pattern can also be clearly observed for Segments $\#4$ and $\#6$, during which the person also slept on his back. For the Segment $\#3$ (slept at the left side) and the Segment $\#5$ (slept at the right side), the periodicity vectors have different and distinct patterns. These periodicity vectors will be compared with those in a topography database built a priori to identify sleeping position.

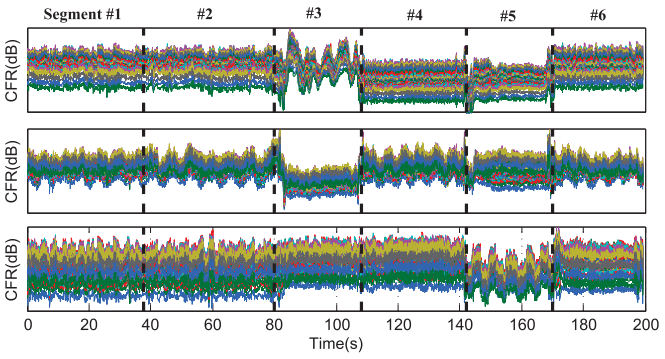

Fig. 22. The measured CSI data segmented using the obtained change points. Compared to Fig. 19, there is one 'false-positive' change point located near 40s.

4.5 Tracking Abnormal Breathing

In this section, we describe how to identify the abnormal respiration, in particular, the sleep apnea. We did a number of experiments during which the test subject was holding his breathing for about 10 seconds. Fig. 25a shows the

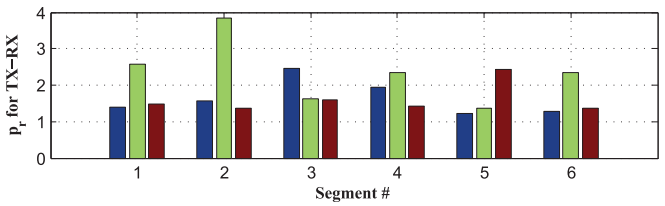

Fig. 24. The finally obtained periodicity vector for each segment of data.

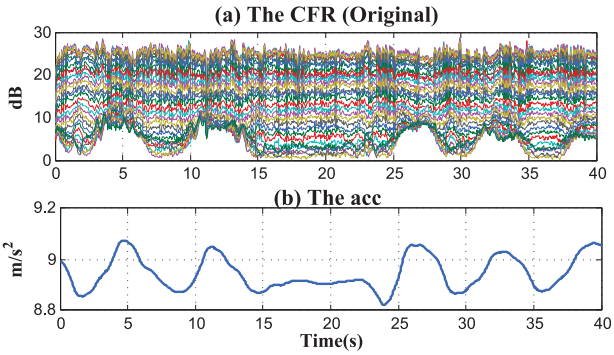

Fig. 25. (a) The original 30 CFR sequences. (b) The corresponding acceleration data.

originally obtained CFR sequences of 30 sub-carriers from the TX1-RX2 pair. Fig. 25b shows the acceleration data recorded at the same time. From the acceleration data, we can briefly observed that the 'sleep apnea' starts from about 15 seconds and ended at 25 seconds.

Our objective is to detect the sleep apnea using the CFR sequences. From Fig. 25, we can roughly observe that in the presence of sleep apnea, all the 30 CFR sequences become stable. This indicates that if we find the CFR sequences are initially periodic but then become stable at a certain time, then an apnea occurs. However, as can be seen in Fig. 19, change of sleeping position can also cause the similar effect. Therefore, we must identify whether the loss of periodicity in CFR sequences are caused by the sleep apnea or by the change of sleeping positions.

We devise the following approach to detect sleep apnea, which is similar to the posture identification described in Section 4.4. First, the CFR data are pre-processed (described in Section 4.2), followed by the change point detection and segmentation (described in Section 4.4.3). As an example, Fig. 26a shows the pre-processed CFR data (shown as blue curves), the change points for each of the 30 sub-carriers (shown as red dots), and the finally obtained three segments (separated by the two dashed vertical lines).

Each data segment may correspond to several conditions: normal breathing in different sleeping positions, or the sleep apnea. As was done in detecting sleeping positions, we still adopt the periodicity level of the CFR sequences as the feature to detect sleep apnea. This is based on the observation that while during normal breathing, one or more TX-RX pairs will show high periodicity level, the CFR sequences from all TX-RX pairs during a sleep apnea will have low periodicity level.

As an illustration, Fig. 26b shows the periodicity level of all 30 sub-carriers of TX1-RX2 for the three data segments shown in Fig. 26a. We can see that for segments #1 and #3 that correspond to normal breathing, some sub-carriers, especially those after #20, show high periodicity level. While for segment #2 which corresponds to sleep apnea, the periodicity level of all 30 sub-carriers are relatively low. Furthermore, Fig. 26c shows the periodicity level for all the three TX-RX pairs in these three data segments. The result matches well with our observation.

To give accurate estimation of the sleep apnea, we extend the PET method proposed in Section 4.4.2 by incorporating the periodicity signature of typical sleep apnea into the tomography database.

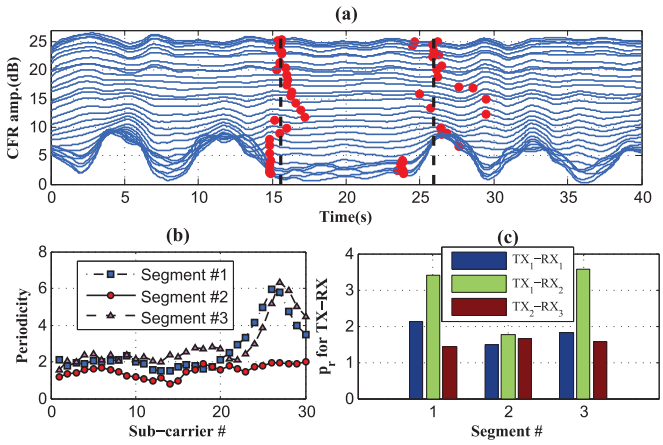

Fig. 26. (a) The processed CFR sequences, with the change points identified for each CFR sequence. The dashed vertical lines are the finally obtained change points using the DBSCAN method. (b) The periodicity level of all sub-carriers of TX1-RX2 for the three segments. (c) The periodicity level of three TX-RX pairs for the three segments.

5 Experiments and Evaluation

5.1 Implementation, Experimental Methodology, and Evaluation Metrics

We prototype our system with commodity WiFi devices and evaluate its performance in a typical office. Two commercial TP-LINK WR740 wireless routers, denoted as TX_1 and TX_2, are employed as the transmitters operating in IEEE 802.11n AP mode at 2.4 GHz. Two Dell M2300 desktop computers, denoted as RX_1 and RX_2, are used as receivers, which is equipped with off-the-shelf Intel 5300 NIC. The transmitter TX_1 is programmed to broadcast packages to RX_1 and RX_2 every 50 ms, and TX_2 is programmed to send packages to RX_3 with the same rate. The data will be processed by the corresponding laptop. In the meantime, the ground-truth respiration is obtained by a smartphone attached to the person's chest.

We will evaluate our system in three aspects: (1) Monitoring normal breathing with known and fixed sleeping positions, (2) monitoring normal breathing under the change of sleeping positions, and (3) monitoring abnormal breathing (i.e., sleep apnea) with fixed sleeping positions. In addition, we also inspect the impacts of various factors, including window size of each segment, and the distance between the TX and RX.

The evaluation metrics are described as follows.

1. Accuracy of respiration rate estimation

Let the respiration rate estimated based on a segment of CFR sequences be f_{CFR}, and the 'true' respiration rate estimated by the smartphone accelerometers be f_{ACC}, then we define the respiration rate is correctly identified if $f_{CFR} \in [0.9f_{ACC}, 1.1f_{ACC}]$. For a test in which we have N segments of CFR data, we define the accuracy of respiration rate estimation, denoted as $RR = m/N$, as the final metric for respiration estimation, where m is the number of the segments for which the respiration rate are successfully identified.

2. Change point detection

To evaluate the performance of change point detection, we record the occurrence time of every real change (including change of sleeping positions and sleep apnea). Denote the time as t_{CHG}, if we find that the time of change point

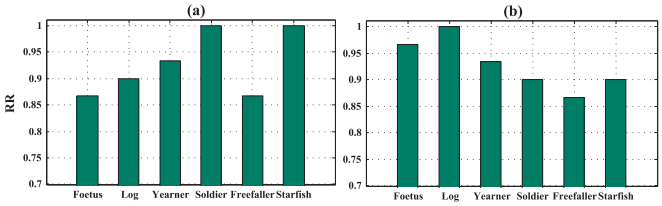

Fig. 27. The accuracy of respiration rate estimation under different sleeping positions using data from (a) TX_1-RX_2 and (b) TX_1-RX_1. The results show that using data from TX_1-RX_2, the respiration can tracked very well when the person is sleeping on his back (i.e., 'Soldier' and 'Starfish'), while using data from TX_1-RX_1 can work well when the person is sleeping on one side (i.e., 'Foetus','Log', and 'Yearner').

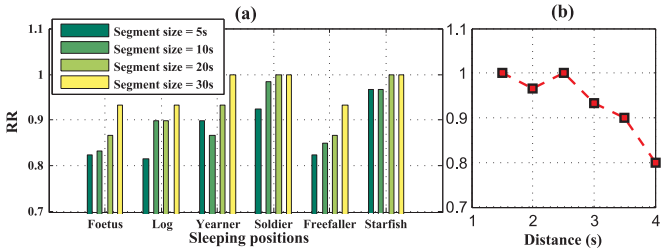

Fig. 28. (a) The impact of window size for respiration rate estimation under different sleeping positions using data from TX_1-RX_2. We can see that in most conditions, a longer window size can improve the accuracy of respiration rate estimation. (b) The impact of distance between the TX and RX pair.

estimated by the sliding window method, denoted as t_{SLID}, satisfies $t_{SLID} \in [t_{CHG} - 2s, t_{CHG} + 2s]$, then we declare that this change point is correctly identified.

3. Estimation of sleeping positions and sleep apnea

We utilize the confusion matrix to evaluate the performance of our system in estimating sleeping positions and sleep apnea. In particular, for each segment of CFR sequences, we will identify the corresponding state of the person. The state falls into one of the following four categories:

- A: Sleeping on the back, breathing normally,
- B: Sleeping on the left side, breathing normally,
- C: Sleeping on the right side, breathing normally, and
- D: Sleep apnea.

5.2 Performance

5.2.1 Performance of Monitoring Normal Breathing with Known and Fixed Sleeping Positions

We first test the system's performance when the person is at fixed six sleeping positions shown in Fig. 14. For each position, the test lasts about 10 minutes and the person is taking normal breathing. For convenience, we let the person always sleep at his left side for positions including 'Foetus', 'Log' and 'Yearner'. Therefore, only data from TX_1-RX_1 and from TX_1-RX_2 will be utilized in this experiment.

First, we let the window size for respiration estimation to be 20 seconds. Therefore, the CFR sequences in the test is divided into 30 segments. Figs. 27a and 27b show the RR for the six sleeping positions using data from TX_1-RX_2 and TX_1-RX_1, respectively.

First, we can observe that generally speaking, our system can reliably track the respiration rate for different sleeping positions. Both TX_1-RX_2 and TX_1-RX_1 can give high estimation rate (greater than 85 percent) for all the six sleeping positions. The high accuracy can be partially attributed to the fact that information from all of the 30 sub-carriers has been efficiently utilized.

Second, it can be seen that when the person is sleeping on his back (e.g., 'Soldier' and 'Starfish'), TX_1-RX_2 performs very well. The respiration rate for all the 30 segments are correctly identified with $RR = 1$. When the person is sleeping on his left side, the RR of using TX_1-RX_2 is a little bit lower. On the other hand, Fig. 27b shows the results using data from TX_1-RX_1. We can see that using data from TX_1-RX_1, the person's respiration can be accurately monitored for 'Foetus', 'Log', and 'Yearner'. The results match well with our observations described in Section 4.4.1. Therefore, if we can accurately identify the sleeping positions, it is expected that one's respiration can be accurately monitored.

The impact of window size

We evaluate the impact of the size of the segments for respiration monitoring. Fig. 28a shows the accuracy of respiration rate estimation under four different window size, 5s, 10s, 20s and 30s. We evaluate the performance under different sleeping positions using data from TX_1-RX_2. We can see that generally speaking, a longer window size can improve the accuracy of respiration rate estimation. Moreover, even when the window size is 5s, using data from TX_1-RX_2 can still accurately estimate the respiration rate (with accuracy greater than 80 percent).

The impact of distance of the TX-RX pair

In previous tests, the distance of the TX_1-RX_2 pair is about 1.5 m. We carried out a number of tests when the TX-RX pair are placed with different distances. In these tests, we fixed sleeping positions to be 'sleep on the back' and let the volunteer to breathing normally. We gradually increase the distance of the TX_1-RX_2 from 1.5 m to 4 m, with the increase of 0.5 m each time. The window size is 20 s. Fig. 28b shows the results for different distances. We can see that the distance between the RX and TX does affect the performance of the respiration monitoring. Generally speaking, a shorter distance between TX and RX can generally achieve higher accuracy. In addition, our system can still achieve more than 80 percent accuracy even when the distance between the TX and the RX is 4 m.

5.2.2 Change Point Detection for Change of Sleeping Positions and Sleep Apnea

We carried out two experiments to test the performance of our system in identifying change points in CFR sequences.

The first experiment is associated with detecting change of sleeping positions. The test last for 15 minutes, and during which the test subject stayed in a position for about $20 \sim 30$s, and then turned over quickly (in approximately 1 second) to another one. The total number of changes of sleeping position is 60. These change of positions can be divided into six types: A→B, B→A, A→C, C→A, B→C and C→B. Then we use the sliding window method proposed in Section 4.4.2 to find out the time instants when the person changed his positions. Table 3 shows the corresponding results. For example, 10 out of 12 position changes from A→B are correctly identified, indicating the success rate to be 83.3 percent. It can be seen that over 80 percent change points have been successfully detected. In addition, Table 3 also shows

TABLE 3
The Results of Detecting Change of Positions

Type of changing positions	Total times	Correctly identified times	Success rate(%)
A → B / B → A	12/12	10/11	83.3/91.6
A → C / C → A	10/10	8/9	80/90
B → C / C → B	8/8	8/7	100/87.5
Types of positions	Number of state	Correctly segmented	Success rate(%)
A	24	19	79.1
B	21	19	90.5
C	18	16	88.9

the results of segmentation based on the identified change points. For example, 19 out of 24 data segments belonging to position A are correctly identified. For position B and C, the success rates are 90.5 and 80.9 percent, respectively.

The second test is associated with detecting change points caused by sleep apnea. The test last for 30 minutes, and the test subject was sleeping on this back and hold his breath from time to time. The ground truth of change points in the test is recorded by the observer.

In this test, there are a total of 56 breathing pauses. Regarding the start time of these breathing pauses, the sliding window method successfully identified 49 out of 56 start points. There are also nine false positives which do not correspond to any of the actual breathing pauses. With respect to the end time of the breathing pauses, 46 out of 56 end points are identified, with five false positives. To summarize, there are 46 out of the 56 breathing pauses are correctly identified, and the detection rate is about 82.1 percent.

5.2.3 Estimation of Sleeping Positions and Sleep Apnea

In this section, we test the performance of the system to identify four different states of a sleeper.

In particular, the training data sets for normal breathing are obtained by letting a person stay in three designed positions (back, left side and right side), each position for 15 minutes. In addition, we also collected the 15-minute data when the person hold the breath (sleep apnea). Then these 15-minute data for each state are evenly divided into 20 data segments. For each data segment, a periodicity vector is obtained. Thus we can build a topography database for three sleeping postures and the sleep apnea. Note that in order to demonstrate the generality of the PET, the training data sets are collected based on a different person from the testing data.

We utilize the data described in Section 5.2.2 as the testing data. Given a newly obtained data segment from the testing data, we first calculate its periodicity vector, and the compared to the database. The data set in the database with the maximum similarity provides the state of the sleeper for the testing segment. Table 4 shows the confusion matrix for the actual and estimated sleeping positions. For example, among the 24 data segments belonging to position A, 22 are correctly identified as A, while two are erroneously identified as position B. The accuracies for the positions A, B, C, D are 91, 85.8, 88.9, and 93.5 percent, respectively.

TABLE 4
The Confusion Matrix for the State Estimation

Actual Estimated	A	B	C	D	Total	Accuracy
A	22	2	0	0	24	91%
B	1	18	2	0	21	85.7%
C	0	1	17	0	18	88.9%
D	2	1	0	43	46	93.5%

6 Limitations and Future Work

In this paper, we introduce how to take wireless signals collected from off-the-shelf WiFi devices in bedrooms as 'sensors' to monitor a person's sleep. The preliminary results show that fine-grained sleep information like a person's respiration, sleeping postures and rollovers can be reliably extracted.

Here, we discuss some limitations of the current work and the problems that deserve in-depth study in the future. First, to simulate sleep apnea, we let awake volunteers to hold their breath. The chest movement in this condition can be different from real sleep apnea. Second, we only utilize data collected from two different volunteers, one for establishing the database and the other for the testing data. The generality of our system for different sleepers has not been investigated thoroughly.

There are many interesting problems that deserve in-depth study. For example, can the CSI help to identify activities like hand movements? Can we still be able to extract one's respiration in the presence of these activities? Can we monitor multiple persons' breath simultaneously? We are working on these questions and hope to obtain some satisfactory results in near future.

Acknowledgments

This research is financially supported in part under the NSF of China with Grant 61572218, 61572217, 62172053, 61332004, and NSFC/RGC Joint Research Scheme (3-ZG1L).

References

[1] F. P. Cappuccio et al., "Quantity and quality of sleep and incidence of type 2 diabetes a systematic review and meta-analysis," *Diabetes Care*, vol. 33, no. 2, pp. 414–420, 2010.
[2] C. Iber et al., *The AASM Manual for the Scoring of Sleep and Associated Events: Rules, Terminology and Technical Specifications*. Darien, IL, USA: American Academy of Sleep Medicine, 2007.
[3] (2014). Tanita [Online]. Available: https://www.tanita.co.jp/products/models/sl501.html/
[4] (2014). Philips vital signs camera [Online]. Available: http://www.vitalsignscamera.com/
[5] C. Li, J. Ling, J. Li, and J. Lin, "Accurate doppler radar noncontact vital sign detection using the RELAX algorithm," *IEEE Trans. Instrum Meas.*, vol. 59, no. 3, pp. 687–695, Mar. 2010.
[6] J. Salmi and A. F. Molisch, "Propagation parameter estimation, modeling and measurements for ultrawideband MIMO radar," *IEEE Trans. Antennas Propag.*, vol. 59, no. 11, pp. 4257–4267, Nov. 2011.
[7] R. Ruth, S. Elliot, C. Ke-Yu, G. Mayank, G. Sidhant, and S. N. Pate, "Wibreathe: Estimating respiration rate using wireless signals in natural settings in the home," in *Proc. IEEE Int. Conf. Pervasive Comput. Commun.*, 2015, pp. 131–139.
[8] F. Adib, H. Mao, Z. Kabelac, D. Katabi, and R. C. Miller, "Smart homes that monitor breathing and heart rate," in *Proc. 33rd Annu. ACM Conf. Human Factors Comput. Syst.*, 2015, pp. 837–846.

[9] F. Adib, Z. Kabelac, H. Mao, D. Katabi, and R. C. Miller, "Demo: Real-time breath monitoring using wireless signals," in *Proc. 20th Annu. Int. Conf. Mobile Comput. Netw.*, 2014, pp. 261–262.
[10] N. Patwari, J. Wilson, S. Ananthanarayanan, S. K. Kasera, and D. R. Westenskow, "Monitoring breathing via signal strength in wireless networks," *IEEE Trans. Mobile Comput.*, vol. 13, no. 8, pp. 1774–1786, Aug. 2014.
[11] N. Patwari, L. Brewer, Q. Tate, O. Kaltiokallio, and M. Bocca, "Breathfinding: A wireless network that monitors and locates breathing in a home," *IEEE J. Select. Topics Signal Process.*, vol. 8, no. 1, pp. 30–42, Feb. 2014.
[12] O. J. Kaltiokallio et al., "Non-invasive respiration rate monitoring using a single COTS TX-RX pair," in *Proc. 13th Int. Symp. Inf. Process. Sens. Netw.*, 2014, pp. 59–70.
[13] H. Abdelnasser, K. A. Harras, and M. Youssef, "UbiBreathe: A ubiquitous non-invasive WiFi-based breathing estimator," in *Proc. 16th ACM Int. Symp. Mobile Ad Hoc Netw. Comput.*, 2015, pp. 277–286.
[14] J. Paalasmaa, M. Waris et al., "Unobtrusive online monitoring of sleep at home," in *Proc. Annu. Int. Conf. IEEE Eng. Med. Biol. Soc.*, 2012, pp. 3784–3788.
[15] C. Scully, L. Jinseok, J. Meyer, A. M. Gorbach, D. Granquist-Fraser, Y. Mendelson, and K. H. Chon, "Physiological parameter monitoring from optical recordings with a mobile phone," *IEEE Trans. Biomed. Eng.*, vol. 59, no. 2, pp. 303–306, Feb. 2012.
[16] Z. Yang, Z. Zhou, and Y. Liu, "From RSSI to CSI: Indoor localization via channel response," *ACM Comput. Surveys*, vol. 46, no. 2, p. 25, 2013.
[17] L. Davies and U. Gather, "The identification of multiple outliers," *J. Am. Statist. Assoc.*, vol. 88, no. 423, pp. 782–792, 1993.
[18] J. D. Villasenor, B. Belzer, and J. Liao, "Wavelet filter evaluation for image compression," *IEEE Trans. Image Process.*, vol. 4, no. 8, pp. 1053–1060, Aug. 1995.
[19] A. V. Oppenheim, R. W. Schafer, J. R. Buck et al., *Discrete-Time Signal Processing*, vol. 2. Englewood Cliffs, NY, USA: Prentice-Hall, 1989.
[20] B. Iglewicz and D. C. Hoaglin, *How to Detect and Handle Outliers*, vol. 16. Milwaukee, WI, USA: ASQ Quality Press, 1993.
[21] J. C. Lagarias et al., "Convergence properties of the nelder–mead simplex method in low dimensions," *SIAM J. Optim.*, vol. 9, no. 1, pp. 112–147, 1998.
[22] Sleep position gives personality clue. BBC News 2003, [Online]. Available: http://news.bbc.co.uk/2/hi/health/3112170.stm
[23] R. Kirk, *Statistics: An Introduction*. Boston, MA, USA: Cengage Learning, 2007.
[24] V. V. Petrov, *Limit Theorems of Probability Theory*. Oxford, U.K.: Clarendon Press, 1995.
[25] M. Ester, H.-P. Kriegel, J. Sander, and X. Xu, "A density-based algorithm for discovering clusters in large spatial databases with noise.," in *Proc. 2nd Int. Conf. Knowl. Discovery Data Mining*, 1996, vol. 96, pp. 226–231.

Xuefeng Liu received the MS and PhD degrees from the Beijing Institute of Technology, China, and the University of Bristol, United Kingdom, in 2003 and 2008, respectively. He is currently working in the School of Information and Electronics, Beijing Institute of Technology, China. His research interests include wireless sensor networks and in-network processing. He has served as a reviewer for several international journals/conference proceedings.

Jiannong Cao received the MSc and PhD degrees in computer science from the Washington State University, Pullman, Washington, in 1986 and 1990, respectively. He is currently the head and chair professor in the Department of Computing, Hong Kong Polytechnic University, Hong Kong. His research interests include parallel and distributed computing, networking, mobile and wireless computing, fault tolerance, and distributed software architecture. He is a fellow of the IEEE.

Shaojie Tang received the PhD degree in computer science from the Illinois Institute of Technology in 2012. He is currently an assistant professor in the Naveen Jindal School of Management, University of Texas, Dallas. His research interest includes social networks, game theory, e-business, and optimization. He served as chairs and TPC members at numerous conferences.

Jiaqi Wen received the bachelor's degree from the Sun Yat-Sen University, Guangzhou, China, in 2013. He is currently working toward the MPhil degree in the Department of Computing, Hong Kong Polytechnic University. His research interests include wireless sensor networks and activity recognition.

Peng Guo received the MS and PhD degrees from the Huazhong University of Science and Technology, Wuhan, China, in 2003 and 2008, respectively. He is currently an associate professor in the School of Electronics and Information Engineering, Huazhong University of Science and Technology. His research interests include wireless sensor networks, distributed computing, and in-network processing.